Available online at www.sciencedirect.com
SCIENCE DIRECT®
Journal of Photochemistry and Photobiology A: Chemistry 162 (2004) 153–162
Journal of Photochemistry and Photobiology A:Chemistry
www.elsevier.com/locate/jphotochem

Photochemistry of sulfosalicylic acid in aqueous solutions

Ivan P. Pozdnyakov [a], Victor F. Plyusnin [a,*], Vjacheslav P. Grivin [a], Dmitry Yu. Vorobyev [a], Aleksandr I. Kruppa [a], Helge Lemmetyinen [b]

[a] *Institute of Chemical Kinetics and Combustion Photochemistry, Institutskaya 3, 630090 Novosibirsk, Russia*
[b] *Institute of Materials Chemistry, Tampere University of Technology, P.O. Box 589, 33101 Tampere, Finland*

Received 17 June 2003; received in revised form 10 July 2003; accepted 14 July 2003

Abstract

Nanosecond laser flash photolysis (XeCl, 308 nm), optical spectroscopy, fluorescence, and time-resolved chemically induced nuclear polarization (CIDNP) were used to determine photophysical and photochemical processes for 5-sulfosalicylic acid dianion ($HSSA^{2-}$) in aqueous solutions and frozen matrices. The triplet–triplet absorption (TTA) band with a maximum at 470 nm was recorded under excitation in the region of the long-wave absorption band of dianion ($\lambda_{max} = 300$ nm). For high laser pulse intensities, a two-quantum formation of an aquated electron is observed. CIDNP in solutions and flash photolysis in frozen matrices, with preliminary excitation to populate T_1 state, indicate that photoionization occurs during absorption of a second quantum by an excited singlet S_1 state. The spectral and kinetic characteristics of the excited states of dianion and aquated electron were determined.

Keywords: Sulfosalicylic acid; Laser flash photolysis; Triplet–triplet absorption; Two-quantum processes; Aquated electron

1. Introduction

Organic acids (R-CO_2H) are a class of compounds abundant in natural water [1]. The main source of organic acids is the digestion of residual plants by microorganisms in water and soil. These acids can form complexes with many transient metals whose photochemistry can contribute substantially to the balance of organic compounds in water [2–6]. To determine the processes initiated by solar radiation in natural water, it is necessary to study primary photochemical reactions for coordination compounds [7,8] including those with oxyacids as ligands. It is important to note, however, that aromatic acids have their own strong absorption bands in UV range and can be subjected to photochemical transformations under solar radiation in a free noncoordinated state.

Salicylic acid (2-hydroxybenzoic acid) (SA) and its derivatives (SAD) belong to aromatic oxyacids family and can serve as model compounds, which demonstrate the photochemical properties of natural oxyacids. SA and SAD are known to luminescence in the blue spectrum range [9,10–12]. However, the photophysical and photochemical properties of these molecules are poorly characterized. It was not until recently that the spectrum of triplet–triplet absorption (TTA) of SA in organic solvents recorded by laser flash photolysis was published [11]. The photochemical and photophysical processes have been studied for 5-sulfosalicylic acid (SSA) in aqueous solutions in the framework of the program for studying photochemical transformations of various compounds in natural water. SSA was used because of its better solubility in water as compared with SA. The spectral and kinetic characteristics of primary intermediate states and species are examined in the study.

2. Experimental details

We employed a set-up for laser flash photolysis using excimer XeCl laser excitation (308 nm) with a pulse duration of 15 ns and a mean pulse energy of 20 mJ. For details see [13]. The spectrum and kinetics of SSA fluorescence were measured on a PRA spectrofluorimeter with photon counting. The optical spectra were recorded using an HP 8453 "Hewlett Packard" spectrophotometer.

In the numerical calculations of the kinetic curves of the appearance and disappearance of intermediate optical absorption, differential equations were solved by a special program using the fourth-order Runge–Kutta method. The laser pulse power was estimated using solutions of anthracene in benzene. The TTA of anthracene in this solvent at $\lambda = 431$ nm has the absorption coefficient $\varepsilon = 42{,}000\ M^{-1}\ cm^{-1}$ for the quantum yield of formation $\varphi = 0.53$ [14].

* Corresponding author. Tel.: +7-3832-332385; fax: +7-3832-342350.
E-mail address: plyusnin@ns.kinetics.nsc.ru (V.F. Plyusnin).

1010-6030/$ – see front matter © 2004 Elsevier B.V. All rights reserved.
doi:10.1016/S1010-6030(03)00341-1

SSA (Aldrich) and 2,2′-dipyridyl (DP; Aldrich), as a triplet energy acceptor, were employed without repurification. Doubly distilled water was used to prepare solutions. All experiments were carried out in oxygen-free solutions. Oxygen was removed by bubbling solutions with gaseous nitrogen. Aqueous 4 M $Mg(ClO_4)_2$ solutions, which form at 77 K the transparent glassy matrices, were used to study processes at low temperatures.

The effects of time-resolved photo-chemically induced nuclear polarization (CIDNP) were determined on a set-up based on an NMR DPX-200 Bruker spectrometer and excimer Lambda Physik EMG-101 (XeCl, 100 mJ, pulse duration: 15 ns) laser [15]. The optical part of the set-up supplied ∼25% of laser energy to a sample.

3. Results and discussion

3.1. Optical spectra of SA and SSAs

The optical absorption spectra of SA and SAD are determined by the π-system of an aromatic ring interacting with an additional π-bond on the C=O group of an acid residue. Indeed, if the benzene absorption band is centered to 250 nm, in aqueous solutions, SA has a fairly strong absorption band at 300 nm ($\lambda_{max} = 303$ nm, $\varepsilon = 3500\ M^{-1}\ cm^{-1}$) [16,17]. Introducing substituents into SA red-shifts the absorption band [9].

The fluorescent properties of SA and SAD have been studied in a series of polar (water, ethanol, dimethylformamide, chloroform) and nonpolar solvents (benzene, *n*-heptane, isooctane, methylcyclohexane). In the ground state, there is a strong intramolecular hydrogen bond between carboxyl and hydroxyl SA groups. A fast (60 fs [11]) intramolecular proton transfer giving rise to a tautomer form occurs upon SA excitation. This accounts for a large Stokes shift of SA fluorescence band and its derivatives. In polar aprotic and nonpolar solvents, the fluorescence band maximum is observed at 450 nm [9,10,12]. For proton polar solvents, such as water and ethanol, the fluorescence band maximum for SA and SAD moves to a short-wave range (400 nm) with an increase in lifetime (from 1 to 6–8 ns) and fluorescence quantum yield [9]. This is due to proton transfer to a solvent in the ground state, which results in the formation of an anion of the corresponding acid whose photophysical parameters differ from the characteristics of a neutral molecule.

Fig. 1 shows the optical SSA spectra in aqueous solutions with different pH. SSA has three acid protons (H_3SSA) that can dissociate in aqueous solutions. The SO_3H group proton dissociates over a wide pH range (0–14) for COOH and OH groups, $pK = 2.9$ and 11.8, respectively [18]. Over the pH range from 0 to 10, there are actually no considerable changes in absorption spectrum due to the similar parameters of the spectra of H_2SSA^- and 5-sulfosalicylic acid dianion ($HSSA^{2-}$) ions. These particles display a

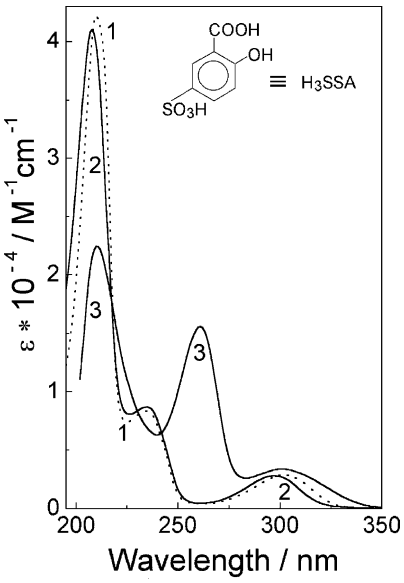

Fig. 1. Optical absorption spectra of SSA ions in aqueous solutions at 298 K. (1) H_2SSA^- monoanion ($HClO_4$, pH = 1); (2) $HSSA^{2-}$ dianion (NaOH, pH = 10); (3) SSA^{3-} trianion (NaOH, pH = 13).

long-wave absorption band with a maximum at 300 nm with an extinction coefficient of about $2800\ M^{-1}\ cm^{-1}$. In the far UV range, there are two absorption bands with maxima at 235 nm ($\varepsilon = 8500\ M^{-1}\ cm^{-1}$) and 210 nm ($\varepsilon = 41{,}000\ M^{-1}\ cm^{-1}$). At high pH (≥12), the optical spectrum exhibits a new absorption band with a maximum at 260 nm ($\varepsilon = 14{,}200\ M^{-1}\ cm^{-1}$), which corresponds to acid trianion (SSA^{3-}). Thus, in aqueous solutions, over a wide pH range (4–10), the SSA is in the form of dianion $HSSA^{2-}$ whose photophysics and photochemistry are described in this paper.

3.2. Laser flash photolysis of aqueous solutions of dianion $HSSA^{2-}$

Excitation of the oxygen-free aqueous solutions of dianion $HSSA^{2-}$ by a laser pulse (308 nm) gives rise to intermediate absorption consisting of three bands with maxima at 310, 470, and 720 nm (Fig. 2a). The bands at 470 and 720 nm decay at substantially different rates (Fig. 2b), which indicate the formation of several intermediate species after the laser pulse. The band lifetime at 470 nm decreases sharply in the presence of oxygen, which is evidence that the band belongs to $HSSA^{2-}$ absorption from the triplet state. The TTA band of a neutral form of SA in cyclohexane has a maximum at 440 nm [11]. The shift of 30 nm is due to the introduction of a substituent into a ring (SO_3^- group), the change in acid form (neutral SA form and dianion $HSSA^{2-}$), and the use of another type of a solvent (water versus organic solvent).

Based on data from pulse radiolysis, it is known that a wide band with a maximum at 720 nm belongs to the absorption of aquated electron (e_{aq}^-) [19–21]. In Fig. 2a, the dotted line shows the e_{aq}^- spectrum from [19]. The dependence

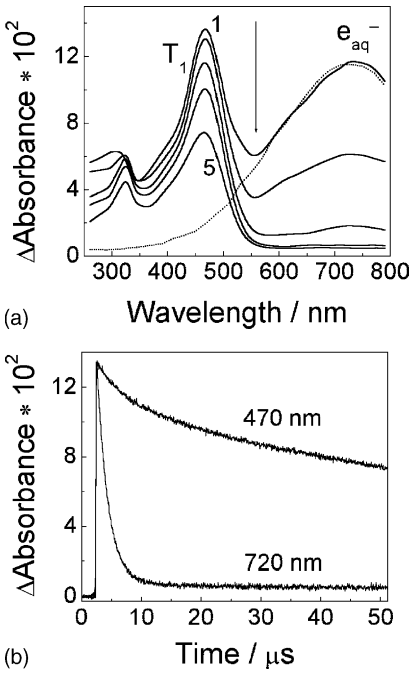

Fig. 2. Laser flash photolysis of aqueous $HSSA^{2-}$ solution (1.5×10^{-4} M). The cell thickness: 1 cm, temperature: 298 K, pH = 10.0, laser pulse intensity: 60 mJ/cm^2. (a) Intermediate absorption spectra (1)–(5): 0, 1.6, 6, 16, and 48 μs after the pulse. The dotted line shows the e_{aq}^- spectrum from [19]. (b) Kinetic curves at 470 and 720 nm.

of the yield of the $HSSA^{2-}$ TTA and e_{aq}^- on laser pulse intensity is shown in Fig. 3. The TTA (470 nm) increases linearly at low intensity and starts to approach saturation with intensity exceeding 100 mJ/cm^2. The e_{aq}^- absorption

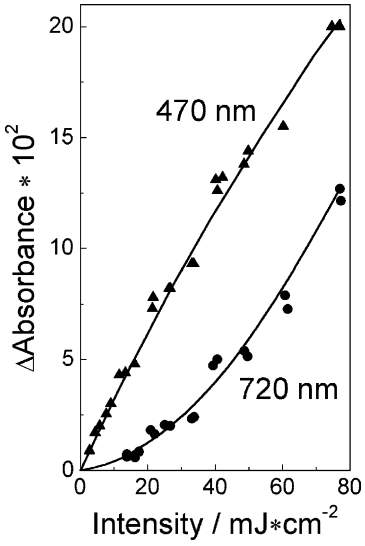

Fig. 3. Dependence of the optical density of the $HSSA^{2-}$ TTA (470 nm) and e_{aq}^- absorption (720 nm) on laser pulse intensity in aqueous $HSSA^{2-}$ solution (1.2×10^{-4} M) at pH = 10.0. The cell thickness: 1 cm, D_{308} = 0.23, temperature: 298 K. Symbols—experimental data, solid curves—numerical solution of differential equations for reactions (1)–(4) and (10).

yield (720 nm) is small at low intensities of the laser pulse and starts to increase substantially in the region >40 mJ/cm^2. This indicates a two-quantum process of aquated electron formation.

The slope in the initial part of the dependence of the triplet state yield on laser pulse intensity (Fig. 3) determines the product $\varphi(T)\,\varepsilon_T^{470} = (3.0 \pm 0.2) \times 10^3\ M^{-1}\,cm^{-1}$, where ε_T^{470} is the extinction coefficient of the TTA band with a maximum at 470 nm (Fig. 2a). Thus, the quantum yield of the appearance of the triplet state of dianion $HSSA^{2-}$ can be calculated after determination of the ε_T^{470} value.

3.3. The spectrum and kinetics of $HSSA^{2-}$ fluorescence in aqueous solution

The first excited singlet S_1 state is populated during excitation of dianion $HSSA^{2-}$ in the region of the long-wave absorption band (300 nm). For low laser pulse intensities, when the e_{aq}^- yield is small, the S_1 state either relaxes radiatively (k_{ir}) or nonradiatively (k_{nr}) to the ground S_0 state or transfers to the triplet T_1 state (k_{isc}) via intersystem crossing

$$S_0 \xrightarrow{h\nu} S_1 \quad (1)$$

$$S_1 \xrightarrow{k_{ir}} S_0 + h\nu \quad (2)$$

$$S_1 \xrightarrow{k_{nr}} S_0 \quad (3)$$

$$S_1 \xrightarrow{k_{isc}} T_1 \quad (4)$$

The radiative relaxation from S_1 to S_0 is recorded in the form of a short-living luminescence in the blue region. The fluorescence band maximum is located at 404 nm (Fig. 4a). Note that for SA in aqueous solutions at pH = 7, the luminescence maximum is at 405 nm [12] and corresponds to the anion HSA^- emission. Thus, the presence of a (SO_3^- group)

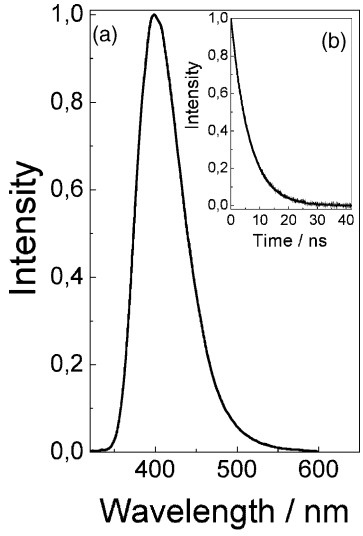

Fig. 4. $HSSA^{2-}$ dianion luminescence in aqueous solution: (a) spectrum; (b) kinetic curve of luminescence disappearance at 400 nm.

in the dianion $HSSA^{2-}$ has almost no effect on the luminescence spectrum. Intersystem crossing to the triplet T_1 state is followed by the appearance of the TTA band with a maximum at 470 nm (Fig. 2a). The lifetime of dianion $HSSA^{2-}$ fluorescence (Fig. 4b) is $\tau_{fl} = 6.3 \pm 0.1$ ns, which determines the sum of the rate constants $1/\tau_{fl} = k_{ir} + k_{nr} + k_{isc} = (1.6 \pm 0.03) \times 10^8\ s^{-1}$.

3.4. Determination of $HSSA^{2-}$ TTA coefficient

The absorption coefficient of the dianion $HSSA^{2-}$ TTA band was determined by the method of triplet–triplet energy transfer. As an acceptor, we used DP with a known TTA spectrum (the band with a maximum at 350 nm and an absorption coefficient of $1.8 \times 10^4\ M^{-1}\ cm^{-1}$ [22]). The weak absorption of DP at 308 nm ($\varepsilon \approx 3 \times 10^2\ M^{-1}\ cm^{-1}$), as compared with $HSSA^{2-}$ absorption ($\varepsilon = 2 \times 10^3\ M^{-1}\ cm^{-1}$), is another reason for the choice of DP as an acceptor. In addition, its weak absorption at 308 nm allows us to directly populate the DP triplet (without $HSSA^{2-}$) and determine its spectral and kinetic parameters.

Indeed, a laser pulse into the aqueous dianion $HSSA^{2-}$ solution with DP is followed by the formation of a new absorption band with a maximum at 350 nm (Fig. 5a). The inset (Fig. 5b) shows the kinetics of optical density change at 470 nm ($HSSA^{2-}$ triplet) and 350 nm (DP triplet). The observed rate constant of $HSSA^{2-}$ TTA disappearance (k_{obs}^{470}) increases with increasing DP concentration. These results confirm the T–T energy transfer. At low laser pulse intensities and small concentrations of $HSSA^{2-}$ triplet, the kinetic curves at 470 and 350 nm can be described by the following scheme:

$$^3HSSA^{2-} + DP \xrightarrow{k_1} {}^1HSSA^{2-}\ (S_0) + {}^3DP \quad (5)$$

$$^3DP \xrightarrow{k_2} {}^1DP\ (S_0) \quad (6)$$

$$^3DP + {}^3DP \xrightarrow{k_3} {}^1DP\ (S_0) + {}^1DP\ (S_1) \quad (7)$$

$$^1DP\ (S_1) \rightarrow {}^3DP \quad (\varphi(^3DP)) \quad (8)$$

The constant $k_1 = (4.2 \pm 0.2) \times 10^9\ M^{-1}\ s^{-1}$ was determined from the dependence of k_{obs}^{470} on the DP concentration. The quantum yield $\varphi(^3DP) = 0.29 \pm 0.02$ and the values for the rate constants $k_2 = (8.1 \pm 1.0) \times 10^3\ s^{-1}$ and $k_3 = (1.7 \pm 0.2) \times 10^9\ M^{-1}\ s^{-1}$ were measured based on the dependence of the yield of DP triplet absorption at 350 nm and value of k_{obs}^{350} on the laser pulse intensity in the absence of $HSSA^{2-}$. The calculated and experimental kinetic curves at 350 and 470 nm obtained for the different initial DP concentrations and with variations in laser pulse intensity were compared to find the absorption coefficient of the $HSSA^{2-}$ TTA band. The system of differential equations was solved for a set of reactions (5)–(8). As fixed parameters, we used the values of constants k_1–k_3, and the ratio between extinction coefficients at 350 and 470 nm for the TTA bands ($\varepsilon_{DP}^{470}/\varepsilon_{DP}^{350} = 0.04$ and $\varepsilon_T^{470}/\varepsilon_T^{350} = 5.0$). The ratio between absorption coefficients was determined from the ratio between the signal amplitudes for the corresponding wavelengths during flash photolysis of the DP and $HSSA^{2-}$ solutions separately. The absorption coefficient of TTA at 470 nm was varied. Its value, $\varepsilon_T^{470} = (6.7 \pm 0.5) \times 10^3\ M^{-1}\ cm^{-1}$, allows us to bring into agreement all calculated and experimental kinetic curves. The solid lines in Fig. 5b show calculations with the above parameters.

The above product $\varphi(T)\ \varepsilon_T^{470}$ and the absorption coefficient were used to calculate the quantum yield of the $HSSA^{2-}$ triplet state, $\varphi(T) = 0.45 \pm 0.05$. The value of the T_1 quantum yield and the S_1 state lifetime make it possible to determine the sum of the constants of radiative and nonradiative $S_1 \rightarrow S_0$ transitions $k_{ir} + k_{nr} = (8.8 \pm 1.0) \times 10^7\ s^{-1}$ and constant of intersystem crossing $k_{isc} = (7.2 \pm 0.7) \times 10^7\ s^{-1}$. Note that for the $HSSA^{2-}$ dianion, the T_1 quantum yield in aqueous solutions exceeds by order of magnitude that for the neutral forms of SA and SSA in organic solvents [11].

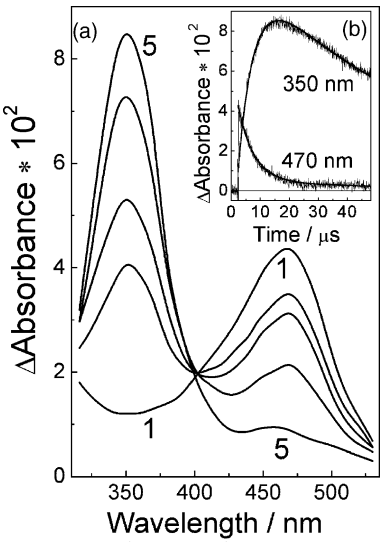

Fig. 5. Determination of the absorption coefficient of $HSSA^{2-}$ TTA band at 470 nm. (a) Intermediate absorption spectra arising from flash photolysis in aqueous solution (pH = 10, temperature: 298 K) of $HSSA^{2-}$ dianion (1.9×10^{-4} M) and DP (5.1×10^{-5} M); (1)–(5): 0, 1.2, 2, 4, and 12 μs after the laser pulse. (b) Kinetic curves at 470 nm ($HSSA^{2-}$ triplet) and 350 nm (DP triplet); solid lines—calculations by the scheme of reactions (5)–(8) with the parameters given in the text.

3.5. Excited state from which the SSA ions are photoionized

The laser pulse duration is 15 ns. Therefore, the $HSSA^{2-}$ dianion absorbing a light quantum during this pulse is first in the excited singlet state (6 ns) and then in the triplet state. Thus, the two-quantum $HSSA^{2-}$ photoionization and e_{aq}^- formation at great laser pulse intensities can occur upon second quantum absorption from both the S_1 and T_1 states.

The time-resolved chemical nuclear polarization method was employed to determine the multiplicity of the state from

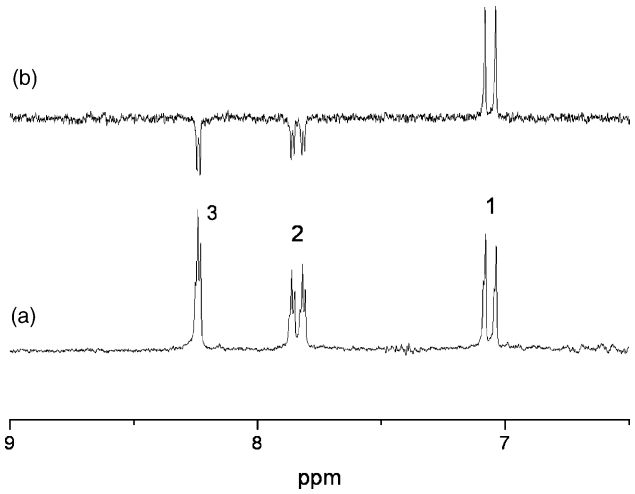

Fig. 6. Determination of the multiplicity of the state of $HSSA^{2-}$ dianion photoionization. ^1H NMR spectra (200 MHz) of 10^{-3} M $HSSA^{2-}$ in water (pH = 10) at 298 K. (a) Initial compound; (b) photo-CIDNP spectrum with 1 μs delay between laser flash and probing pulse. Numbering of proton signals corresponds to structure in Table 1.

which ionization occurs. Fig. 6 shows the CIDNP spectrum recorded during $HSSA^{2-}$ photolysis in D_2O (pH = 10) 1 μs after the laser pulse. This spectrum demonstrates integral polarization on all protons of the primary $HSSA^{2-}$ dianion. The CIDNP effect sign depends on a number of parameters and is commonly given as a simple relation (Kaptein's rule) [23]

$$\Gamma_{net} = \mu\varepsilon\,\Delta g\,a \quad (9)$$

where Γ_{net} describes the net CIDNP effects: $\Gamma_{net} > 0$ corresponds to the absorption and $\Gamma_{net} < 0$ corresponds to emission effects. The other parameters are: $\mu = +1$ for a triplet precursor and $\mu = -1$ for a singlet radical (or ion radical) precursor; $\varepsilon = +1$ for geminate recombination products, and $\varepsilon = -1$ for escape products. Δg is the sign of the g-factor difference between paramagnetic intermediates containing the polarized nuclear and radical partners, a is the sign of the hyperfine coupling constant of a nucleus in the paramagnetic intermediate. In this case, the polarization sign sensitivity to the multiplicity of the geminate pair precursor of $HSSA^{\bullet-}$ radical anion and aquated electron is of importance. When the $HSSA^{2-}$ concentration is $<10^{-3}$ M and the time delay is 1 μs, the polarization observed corresponds mainly to geminate processes, and as a result, $\varepsilon = +1$.

The g-factor of aquated electron in water is 2.002 [24]. In other aqueous solutions and frozen matrices, the value of g-factor for an electron varies from 1.9999 to 2.002 [25], i.e., is smaller than $g_e = 2.0023$ (a free electron g-factor). For the SA radical $HAS^{\bullet}$, $g = 2.00476$ [26], i.e., $g > g_e$ which is typical of many organic radicals and radical ions. If the parameters of the spin Hamiltonian of radical $HAS^{\bullet}$ and $HSSA^{\bullet-}$ are similar, then for $HSSA^{\bullet-}$ we also get $g > g_e$. Therefore, the Δg parameter for the geminate pair of $HSSA^{\bullet-}$ and e_{aq}^- in (9) will be positive.

Table 1
Calculated HFC constants of $HSSA^{\bullet-}$ and CIDNP effects of different protons of $HSSA^{2-}$

Intermediate	Position	Calculated HFC (mT)	CIDNP (rel. int.)
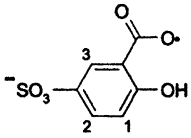	1	−0.876	A (2.02)
	2	0.727	E (1.17)
	3	0.403	E (1.00)

The signs of the HFC constants for the $HSSA^{\bullet-}$ radical anion were calculated as follows: the geometry was optimized by the AM1 method (HyperChem 6); the HFC constants were calculated for optimized geometry using the INDO method (UHF), which was parametrized for calculating magnetoresonance parameters (spin Hamiltonian program) [27]. The calculated results are summarized in Table 1. Taking into account the fact that the nuclear polarization activity is proportional to the value of HFC constant, and the polarization sign depends on the HFC sign, we conclude that although the absolute values of the HFC constant are slightly overestimated, the calculation correctly describes the spin density distribution in the $HSSA^{\bullet-}$ radical anion.

According to the rules of CIDNP effects sign analysis, we conclude that in solution, the polarization observed was formed in the pair of the $HSSA^{\bullet-}$ radical anion and the aquated electron, resulting initially from the singlet state ($\mu < 0$). Thus, the $HSSA^{2-}$ dianion is ionized upon the second quantum absorption by the singlet S_1 state.

Additional data on the multiplicity of the state from which e_{aq}^- is photoionized and formed, were obtained by experiments on flash photolysis of $HSSA^{2-}$ ions in a low-temperature (77 K) glassy matrix (the aqueous 4 M $Mg(ClO_4)_2$ solutions were frozen). Fig. 7a (spectrum 1) shows the optical $HSSA^{2-}$ spectrum in this matrix, which almost coincides with the spectrum in a solution. The stationary photolysis by laser pulses gives rise to the absorption band of the aquated electron with a maximum at 550 nm (Fig. 7a, spectrum 2).

After a laser pulse, the flash photolysis of a low-temperature matrix containing $HSSA^{2-}$ ions, like aqueous solutions, leads to a TTA with a maximum at 470 nm and the aquated electron absorption (a broad band with a maximum at ~620 nm (Fig. 7a, spectrum 3)). A shift of the absorption band maximum of e_{aq}^- to a short-wave spectrum in frozen aqueous solutions of various salts, as compared with liquid water, is typical [19]. The additional shift of maximum of 40–70 nm upon transition from nanosecond time ranges to the long-time ranges is known from the data on pulse radiolysis [19,28,29] and is ascribed to the deepening of a trap in which an electron is localized. It is worth noting that most electrons in a matrix are not stabilized. By the time a stationary spectrum is recorded (~10 s), only 5% of electrons, formed just after the laser pulse, remain. Fig. 7b shows the

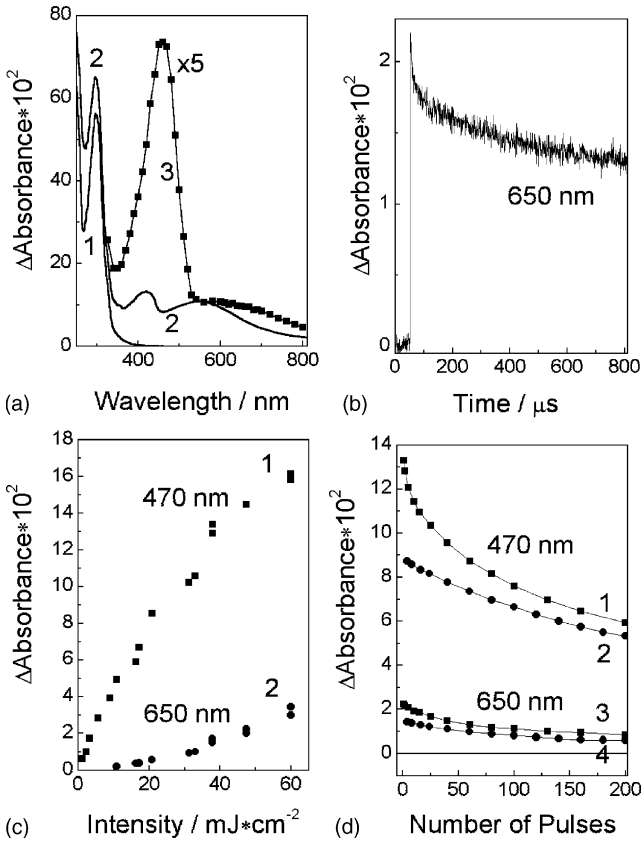

Fig. 7. Photolysis of $HSSA^{2-}$ dianion (3.9×10^{-3} M) in frozen aqueous 4 M $Mg(ClO_4)_2$ solution in the cell of a thickness of 0.049 cm at 77 K. (a) Optical absorption spectra: (1) initial $HSSA^{2-}$ spectrum; (2) the spectrum after 100 laser pulses (10 Hz, 60 mJ/cm^2) recorded 10 s after irradiation; (3) absorption spectrum following laser pulse (increase in five times) upon flash photolysis. (b) Kinetics of the change in optical absorption of an aquated electron at 650 nm. (c) Dependence of the optical density of $HSSA^{2-}$ TTA (470 nm) and e_{aq}^- absorption (650 nm) on laser pulse intensity. (d) A change in the value of TTA at 470 nm ((1) and (2)) and e_{aq}^- absorption at 650 nm ((3) and (4)) during 1 pulse with the total number of pulses absorbed by the sample. (1) and (3)—measurement after each pulse (the time between pulses 10 s); (2) and (4)—upon transfer of a series of 4 pulses to a sample with an interval of 0.1 s (measurement using the last fourth pulse, an interval between the series of 10 s).

nonexponential kinetics of electron absorption disappearance at 650 nm. The complex kinetics probably is due to both the absorption shift to the short-wave spectrum and the electron disappearance in the geminate and bulk recombination with the $HSSA^{\bullet -}$ radical ion involving tunneling [28,29]. The reaction between the e_{aq}^- and the primary $HSSA^{2-}$ ion can make an additional contribution. As illustrated below, in liquid solutions, this reaction substantially determines the kinetics of electron disappearance. In this case, the reaction product is represented by the $HSSA^{\bullet 3-}$ radical ion, and the absorption band with a maximum at 416 nm arising along with e_{aq}^- absorption, can belong to this radical ion (Fig. 7a, spectrum 2).

The yield of triplet and electron absorption in a matrix is also nonlinearly dependent on the laser pulse intensity (Fig. 7c). At 77 K, the lifetime of the triplet state of $HSSA^{2-}$ ions in a matrix reaches ~0.6 s whereas the fluorescence continues to decay in the nanosecond range. The great difference in the lifetimes of T_1 and S_1 states in the frozen matrix was used to determine the multiplicity of the state from which the two-quantum ionization occurs. A considerable portion of $HSSA^{2-}$ ions were transferred into the triplet state by several laser pulses supplied to a sample at 0.1 s intervals (frequency: 10 Hz). A change in absorption at 470 or 650 nm was recorded during the last pulse in a series of pulses. If the T_1 state is the main source of e_{aq}^-, the yield of electrons should increase substantially after preliminary conversion of the $HSSA^{2-}$ ions into this state.

Fig. 7d shows the amplitude of the absorption signals of $HSSA^{2-}$ T_1 state and of e_{aq}^- versus the number of laser pulses absorbed by the sample. The amplitude corresponds to a change of absorbance (ΔD) per pulse. A series of pulses were produced with intervals of 10 s when the triplet state arising from the previous series decayed completely. The value of ΔD is observed to decrease with increasing number of pulses absorbed by the sample because of a decrease in $HSSA^{2-}$ concentration and the accumulation of photolysis products. The governing factor is that the supply of preliminary pulses leads to a decrease in the yield of both the triplet (ΔD_{470}) and the aquated electron (ΔD_{650}). From the value of optical density at 470 nm ($\Delta D_{470} \geq 0.15$ at the beginning of photolysis), we estimate the T_1 state population after three preliminary pulses to the time the registration pulse is supplied. If the absorption coefficient of the TTA band does not change significantly upon transition from solution to frozen matrices, then, taking into account the rate of triplet state decay, approximately 25% of $HSSA^{2-}$ ions are converted into the T_1 state during the three preliminary pulses.

Therefore, the strong CIDNP signal recorded for $HSSA^{2-}$ solutions and a decrease in the aquated electron yield upon transfer of a substantial portion of $HSSA^{2-}$ ions to the triplet state by preliminary pulses in frozen matrices, indicate that for these species, the photoionization occurs upon the second light quantum absorption by the excited singlet S_1 state. $HSSA^{2-}$ in this state is the source of both the e_{aq}^- and the T_1 triplet.

3.6. Two-quantum processes of aquated electron formation

The two-quantum process of electron formation involving the singlet S_1 state can be realized by several ways. Transition from the S_1 state to the highly excited singlet S_N state [30] can cause molecule ionization resulting in a "dry" electron. In aqueous solutions, this electron relaxes in 100–300 fs into the p-state in a trap formed by polarized solvent molecules. By 250–540 fs it is completely stabilized in the ground s-state [31–34]. Electron tunneling from the S_N state into the closely located trap is also possible [35]. The latter process is energetically more advantageous due to

electron transition to the hydrated state. In a frozen matrix, the orientational relaxation of solvent molecules is frozen out. Therefore, an electron can be captured by ready traps only. Since the concentration of these traps close to $HSSA^{2-}$ ions can be low, the electron yield in a low-temperature matrix decreases.

The ionization potential of most benzene derivatives in the gas phase is in the range of 7.5–9.5 eV [36]. In an aqueous medium, ionization potentials are 2–2.5 eV lower due to the interaction of an electron and a cation with the medium [37,38]. Thus, the two-quantum ionization upon absorption of quanta with a wavelength of 308 nm (8.05 eV) can lead to the formation of electrons with energy exceeding the ionization threshold by 0.5–3.0 eV.

The excitation can also be transferred by the $HSSA^{2-}$ ions from the S_N state to a water molecule. The excited water molecules are either ionized with the formation of an $H_2O^{\bullet+}$ radical cation and an electron or, alternatively, dissociate into a hydrogen atom and an $^{\bullet}OH$ radical. In addition to the indirect excitation of water through the S_N state of $HSSA^{2-}$ ions, the direct two-quantum population of the excited state of water molecules is also possible. The existence of these processes is verified by recording the absorption of the aquated electron in pico- and femtosecond experiments on two-quantum ionization of pure water [31–34,39]. However, according to estimates based on the coefficient of two-photon absorption at 308 nm (0.42×10^{-12} m/W [40]), a fraction of absorbed quanta is less than 10^{-3} for a nanosecond pulse ($\tau \approx 15$ ns, $I = 20$–50 mJ) in a 1 cm cuvette. In addition, the nanosecond flash photolysis of pure water indicates the absence of aquated electron absorption.

The mechanism of aquated electron formation, therefore, can be explained by either ionization or by energy transfer to water from the S_N state of the $HSSA^{2-}$ dianion. In [41], the acceptors of an electron (Cd^{2+} ion) and an $^{\bullet}OH$ radical (*n*-butanol) were used to show that the efficiency of energy transfer from the S_N level to water during irradiation of aqueous thymine solutions by picosecond pulses (266 nm) exceeds ionization efficiency by an order of magnitude (quantum yields are 6.5 and 0.65%, respectively). In our study (308 nm), the energy of two-quanta is 1.3 eV lower and the long-wave absorption band of the $HSSA^{2-}$ ion is shifted to the red spectrum by 0.63 eV when compared with thymine. In view of this energy change, the absolute and relative probabilities of both processes can change substantially. For thymine solutions, the laser pulses of picosecond duration are necessary to realize the two-quantum processes due to the short lifetime of the S_1 state (1.2 ps [30]). The fast radiationless processes decrease not only the lifetime but also the quantum yield of thymine fluorescence (10^{-4}). In the case of $HSSA^{2-}$, the long lifetime of the S_1 state (6.3 ns) allows even the nanosecond pulses to initiate the two-quantum processes.

For the two-quantum ionization of pure water by femtosecond pulses at a wavelength of 312 nm with an excess energy of 1.5 eV above the ionization threshold (6.5 eV [42,43]), the mean electron range prior to thermolization is 11–13 Å [39]. This exceeds the Onsager radius for water ($r_c = e^2/\varepsilon kT = 7$ Å at 21 °C) by only 4–6 Å. Under these conditions, about 40% of electrons decay upon geminate recombination of electron and cation in 60–80 ps [39]. The remaining electrons escape into the bulk of the solvent and decay via slower reactions. Thus, the ionization quantum yield at nanosecond times reaches 0.6. In nonpolar solvents with a large Onsager radius ($r_c = 250$–300 Å), almost all electrons formed during two-quantum processes decay upon geminate recombination [44]. In more polar alcohols, 30–50% of electrons escape geminate recombination. This effect depends on excess energy above the ionization threshold. In aqueous solutions, the yield of electrons into the bulk of the solvent increases from 60 to 80% with increasing excess energy from 1.5 to 3.5 eV [30,34,45].

3.7. Optical spectrum, which accompanies aquated electron formation

In the case of $HSSA^{2-}$ ionization, aquated electron formation should be accompanied by the $HSSA^{\bullet-}$ radical anion formation. This species can display an optical absorption spectrum in the nearest UV region. If the process of energy transfer to water contributes significantly to the process of S_N state disappearance, then water ionization gives rise to an aquated electron and a primary $H_2O^{\bullet+}$ radical cation, which rapidly transfers a proton to a water molecule to form an $^{\bullet}OH$ radical. When the amount of transferred energy is insufficient for ionization, the excited water molecule dissociates into an $^{\bullet}OH$ radical and a hydrogen atom. In a geminate reaction with $HSSA^{2-}$ dianion, these particles can form $HSSA(^{\bullet}OH)^{2-}$ and $HSSA(H^{\bullet})^{2-}$ radical ions that can also absorb in the nearest UV region. The rate constant of the reaction between $^{\bullet}OH$ radical and SA ion (HSA^-) is, by an order of magnitude, larger than that of the reaction between a $H^{\bullet}$ atom and this ion (1.2×10^{10} and 1.4×10^9 M^{-1} s^{-1}, respectively [46]). If the relative reactivity of SSA and SA ions is the same, then $HSSA(^{\bullet}OH)^{2-}$ radical ion formation is more probable than $HSSA(H^{\bullet})^{2-}$ formation.

Additional spectrum (except for the spectra of TTA and e_{aq}^-), which should belong to the radical ions of $HSSA^{\bullet-}$ or $HSSA(^{\bullet}OH)^{2-}$, can be determined by comparing absorptions arising at high and low laser pulse intensities. At high laser pulse intensity, the pulse is just followed by $HSSA^{2-}$ in the triplet T_1 state, an aquated electron, and one of these species (radical ions of $HSSA^{\bullet-}$ or $HSSA(^{\bullet}OH)^{2-}$). At low laser pulse intensities, the $HSSA^{2-}$ ion in the triplet state is mainly formed as a result of a drastic decrease in the probability of two-quantum processes. To obtain the additional spectrum, the spectra of e_{aq}^- and of normalized TTA should be subtracted from the total spectrum recorded at high pulse intensity. It is also necessary to take into account a decrease in the $HSSA^{2-}$ dianion absorption (bleaching in the region of the band with a maximum at 300 nm). In the case of $HSSA^{2-}$ ionization from the S_N state, the amount

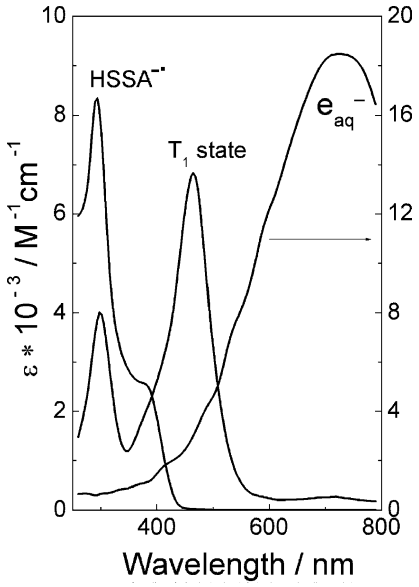

Fig. 8. Optical spectra of intermediate species arising from flash photolysis of aqueous $HSSA^{2-}$ solution (pH = 10). (1) Aquated electron spectrum taken from [19]; (2) TTA spectrum recorded at low laser pulse power. Absorption coefficient is determined from triplet–triplet energy transfer to DP; (3) $HSSA^{\bullet-}$ radical ion spectrum. The method of the production is described in the text.

of decayed dianions in the S_0 state is equal to the sum of the concentrations of the triplet and the aquated electron. Fig. 8 shows the $HSSA^{\bullet-}$ radical anion spectrum calculated by this method. The short-wave band has a maximum at 290 nm and an extinction coefficient of $(8.3 \pm 1.0) \times 10^3\,M^{-1}\,cm^{-1}$. For the long-wave band manifesting itself as a shoulder, the maximum is localized at 380–390 nm and has an extinction coefficient of $(2.5 \pm 0.5) \times 10^3\,M^{-1}\,cm^{-1}$.

If energy transfer to water contributes to the relaxation of the $HSSA^{2-}$ ion S_N state, the spectrum in Fig. 8 will be a superposition of the spectra of $HSSA^{\bullet-}$ and $HSA(^{\bullet}OH)^{2-}$ radical ions. From studies on pulse radiolysis of aqueous solutions of SA, it follows that the $HSA(^{\bullet}OH)^{-}$ radical ion displays an absorption band at 375 nm with the extinction coefficient $\varepsilon = 0.95 \times 10^3\,M^{-1}\,cm^{-1}$ [46]. It is also known that the position of the maxima of radical absorption bands arising from a reaction between an $^{\bullet}OH$ radical and benzoic acid depends weakly on the introduction of a sulfo group as a substituent [47]. Thus, the spectra of $HSSA(^{\bullet}OH)^{2-}$ and $HSA(^{\bullet}OH)^{-}$ radicals can be close to one another and the $HSSA(^{\bullet}OH)^{2-}$ radical ion can make some contribution to the additional absorption is shown in Fig. 8 (the shoulder with a maximum at 380–390 nm). However, according to the values of the absorption coefficients of the shoulder at 380–390 nm of the $HSSA(^{\bullet}OH)^{2-}$ band, this contribution cannot exceed 40%. In addition, the existence of the additional strong band at 290 nm allows us to make the assumption that the $HSSA^{2-}$ ionization from the S_N state, when results in the formation of a $HSSA^{\bullet-}$ radical, is dominant. This conclusion is verified by the presence of the strong CIDNP signal on the $HSSA^{2-}$ protons, which results from the geminate recombination of the $HSSA^{\bullet-}$ radical ion and the aquated electron. It is important to note, that reactions of the radical products of excited water molecule decay should lead to the disappearance of $HSSA^{2-}$ giving no polarization and CIDNP effect.

3.8. Calculations of the dependence of the yield of T_1 state and e_{aq}^- on laser pulse intensity

The data on the dependence of the TTA and e_{aq}^- yields on laser pulse intensity (Fig. 3) can be used to estimate the absorption coefficient of the second quantum absorption from the S_1 state. The exact contribution of energy transfer from the S_N state of the $HSSA^{2-}$ dianion to water remains unknown. Therefore, we assumed it was zero. In this instance, we used reactions (1)–(4) to describe the data on the yield of the T_1 state and e_{aq}^- and took into account the second quantum absorption by the singlet S_1 state followed by $HSSA^{2-}$ ionization from the highly excited S_N state:

$$S_1 \xrightarrow{h\nu} S_N \rightarrow HSSA^{\bullet-} + e_{aq}^- \qquad (10)$$

Comparing the calculated and experimental values for the yield at different laser pulse intensities (Fig. 3), we estimated the product of the absorption coefficient by the ionization quantum yield ($\varphi\,\varepsilon_{S_1}^{308}$). This product will not change even though there is a considerable contribution of energy transfer to water. In this instance, the quantum yield will be only redefined.

The yields were calculated by solving a set of differential equations corresponding to reactions (1)–(4) and (10), and describing the appearance and disappearance of the forming excited states and species. We took into account the total optical density of the sample, the relative fraction of the absorbed light of each species, and the inhomogeneous distribution of the absorbed quanta in the solution. As fixed parameters, we used the constants ($k_{ir} + k_{nr}$) and k_{isc}, the absorption coefficients of the $HSSA^{2-}$ bands in the ground ($\varepsilon_{S_0}^{308}$) and triplet (ε_T^{470} and ε_T^{308}) states, the absorption coefficients of the aquated electron (ε^{720}) and the $HSSA^{\bullet-}$ radical ion (ε_R^{308}). These values have been determined above. The time dependence of laser irradiation intensity was described using the gaussian curve with a width of 15 ns at a half-height. The time range of calculation was 50–100 ns with step in an intervals of 1–10 ps. In Fig. 3 calculation is represented by solid curves. The best agreement between the experimental and calculated data, in terms of the least-squares fit, was obtained for $\varphi\,\varepsilon_{S_1}^{308} = (1.5 \pm 0.3) \times 10^3\,M^{-1}\,cm^{-1}$.

Thus, the minimum absorption coefficient of absorption from the S_1 state is $\varepsilon_{S_1}^{308} \geq 1.5 \times 10^3\,M^{-1}\,cm^{-1}$. If, at times around 50 ns, the ionization quantum yield φ approaches 0.6 due to geminate recombination, then the extinction coefficient $\varepsilon_{S_1}^{308}$ will increase to $2.5 \times 10^3\,M^{-1}\,cm^{-1}$. For a laser pulse intensity of 80 mJ/cm^2 and an initial optical density at

308 nm of 0.23, the e_{aq}^- yield equals approximately 12% of the number of all the quanta absorbed.

3.9. Reactions of the disappearance of T_1 state, e_{aq}^-, and $HSSA^{\bullet -}$ radical anion

In the presence of oxygen, the kinetics of aquated electron disappearance is accelerated substantially due to the high rate constant of reaction of these species ($k = 2 \times 10^{10}\,M^{-1}\,s^{-1}$ for neutral pH [48]). For oxygen concentrations of approximately 2.6×10^{-4} M in water [49], the observed rate constant of e_{aq}^- disappearance should be $5.2 \times 10^6\,s^{-1}$. In other words, the electron should decay within 200 ns. Experiments on the aqueous $HSSA^{2-}$ solutions containing oxygen verified that electron disappearance occurred at 200 ns. Thus, in the presence of oxygen, the main channel of electron disappearance is the reaction

$$e_{aq}^- + O_2 \rightarrow O_2^- \quad (11)$$

In oxygen-free solutions, the e_{aq}^- lifetime increases substantially, which allows us to record other electron reactions. The observed disappearance rate constant (k_{obs}) obtained by treating the kinetic curves of electron absorption disappearance (720 nm) in oxygen-free solutions depends on the initial value of e_{aq}^- absorption and the $HSSA^{2-}$ dianion concentration (Fig. 9a). The slope of the $k_{obs} \propto [e_{aq}^-]$ curves in this figure is due to the reactions

$$e_{aq}^- + e_{aq}^- + 2H_2O \rightarrow 2H^\bullet + 2OH^- \quad (12)$$

$$e_{aq}^- + HSSA^{\bullet -} \rightarrow HSSA^{2-}(S_1) \quad (13)$$

Reaction (13) occurs in the absence of energy transfer to water from the S_N state, otherwise it is necessary to add the reaction between the electron and the $HSSA(^\bullet OH)^{2-}$ radical ion.

Averaging the data from solutions with different $HSSA^{2-}$ concentrations gives the total rate constant $k_{12} + k_{13} = (1.8 \pm 0.3) \times 10^{10}\,M^{-1}\,s^{-1}$. From the experiments on pulse radiolysis of water [48], it follows that $k_{12} = (1.1 \pm 0.14) \times 10^{10}\,M^{-1}\,s^{-1}$. Therefore, for the rate constant of electron recombination with $HSSA^{\bullet -}$ radical we can estimate k_{13} to be $(7.0 \pm 3.0) \times 10^9\,M^{-1}\,s^{-1}$. The cut-off on the ordinate for the straight lines in Fig. 9a depends linearly on the $HSSA^{2-}$ concentration and corresponds to the reaction of electron capture by dianion $HSSA^{2-}$:

$$e_{aq}^- + HSSA^{2-} \rightarrow HSSA^{\bullet 3-} \quad (14)$$

with a rate constant of $k_{14} = (2.7 \pm 0.1) \times 10^9\,M^{-1}\,s^{-1}$, which, with respect to the equal charges of reacting species, is close to the diffusion rate constant.

The characteristic lifetime of the $HSSA^{2-}$ dianion triplet state is, in the presence of oxygen, approximately 1 μs. This lifetime allows us to estimate the constant of triplet state quenching by oxygen, $k_{O_2} = 4.5 \times 10^9\,M^{-1}\,s^{-1}$. This value is close to the diffusion limit in water. In oxygen-free solutions, the kinetics of triplet absorption disappearance is substantially determined by the second-order kinetic law. The linear dependence of the observed constant (k_{obs}) on triplet concentration (Fig. 9b) indicates that the triplet decays mainly as a result of T–T-annihilation

$$^3HSSA^{2-} + {}^3HSSA^{2-} \rightarrow {}^1HSSA^{2-}(S_1) + {}^1HSSA^{2-}(S_0) \quad (15)$$

This reaction results in a dianion $HSSA^{2-}$ in the excited S_1 state that can convert back into a triplet. Taking this effect into account, the slope (Δ) of the straight line in Fig. 9b can be described by the equation

$$\Delta = 2k_{15}\left(1 - \tfrac{1}{2}k_{isc}/(k_{ir} + k_{nr} + k_{isc})\right) = 2k_{15}\left(1 - \tfrac{1}{2}\varphi(T)\right) \quad (16)$$

The quantum triplet yield $\varphi(T)$ has been determined above. Therefore, the data in Fig. 9b can be used to estimate the constant $k_{15} = (6.0 \pm 0.3) \times 10^8\,M^{-1}\,s^{-1}$. The cut-off on the ordinate ($k_{cut} = 4.0 \times 10^3\,s^{-1}$) corresponds to triplet quenching by uncontrolled impurities.

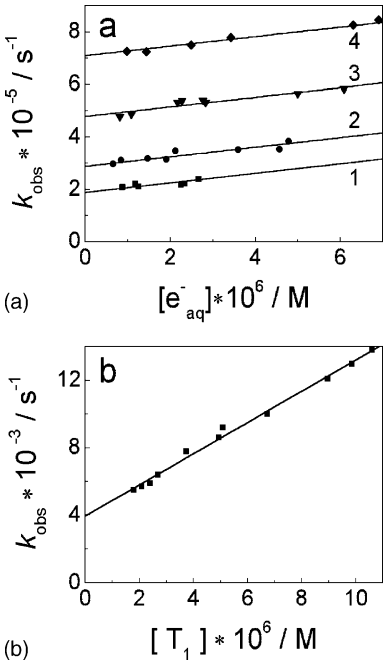

Fig. 9. Observed rate constants (k_{obs}) of the processes of the disappearance of aquated electron and $HSSA^{2-}$ ion T_1 state. The cell thickness: 1 cm, pH = 10.0, temperature: 298 K. (a) Dependence of the k_{obs}^{720} at 720 nm on aquated electron concentration for different $HSSA^{2-}$ concentrations; (1)–(4): $[HSSA^{2-}] \times 10^5 = 3.5$, 6.7, 14.7, and 22 M, respectively. (b) Dependence of the k_{obs}^{470} at 470 nm on the initial concentration of T_1 state for $[HSSA^{2-}] = 1.5 \times 10^{-4}$ M.

4. Conclusions

The laser flash photolysis was used to record the TTA band (470 nm) of the $HSSA^{2-}$ in aqueous solutions. The extinction coefficient of this band was determined using the

triplet–triple energy transfer to DP. We demonstrated that at high laser pulse intensities, an aquated electron forms from two-quantum processes. An analysis of the time-resolved CIDNP effect and the flash photolysis of $HSSA^{2-}$ ions in frozen matrices shows that photoionization occurs upon absorption of second quantum by the excited singlet S_1 state. The rate constants of S_1 state relaxation, and the quantum yields of a triplet and an electron were determined. A comparison of the numerical calculations of the yield of the aquated electron of the TTA with experimental data allowed us to estimate the absorption coefficient of absorption from the S_1 state at a wavelength of 308 nm. The high yield allows us to use the nanosecond laser flash photolysis of $HSSA^{2-}$ in aqueous solutions as a convenient source of an aquated electron.

Acknowledgements

The work was supported by the Russian Foundation for Basic Research (grant nos. N 02-03-032797 and N 03-03-33134) and the Ministry of Education of Russian Federation ("Universities of Russia", UR.05.01.002).

References

[1] E.M. Thurman, Organic Geochemistry of Natural Waters, Martinus Nijhoff/Dr. W. Junk Publisher/Kluwer Academic Publishers, Dordrecht/Boston/Lancaster, 1985, 610 pp.
[2] Y. Zuo, J. Hoigne, Atm. Environ. 28 (1994) 1231–1239.
[3] Y. Zuo, J. Hoigne, Environ. Sci. Technol. 26 (1992) 1014–1022.
[4] B.S. Faust, R.G. Zepp, Environ. Sci. Technol. 27 (1993) 2517–2522.
[5] W. Feng, D. Nansheng, Chemosphere 41 (2000) 1137–1147.
[6] I.P. Pozdnyakov, E.M. Glebov, V.F. Plyusnin, V.P. Grivin, Yu.V. Ivanov, D.Yu. Vorobyev, N.M. Bazhin, Pure Appl. Chem. 72 (2000) 2187–2197.
[7] V. Balzani, V. Carassiti, Photochemistry of Coordination Compounds, Academic Press, London, 1970, 432 pp.
[8] J. Sykora, J. Sima, Photochemistry of Coordination Compounds, Elsevier, Amsterdam, 225 pp.
[9] L. Kozma, I. Khornyak, I. Eroshtyak, B. Nemet, J. Appl. Spec. 53 (1990) 259–265 (in Russian).
[10] P.B. Bisht, M. Okamoto, S. Hirayama, J. Phys. Chem. B 101 (1997) 8850–8855.
[11] H.-C. Ludemann, F. Hillenkamp, R.W. Redmond, J. Phys. Chem. A 104 (2000) 3884.
[12] G.S. Denisov, N.S. Golubev, V.M. Schreiber, Sh.S. Shajakhmedov, A.V. Shurukhina, J. Mol. Struct. 436–437 (1997) 153.
[13] V.P. Grivin, I.V. Khmelinski, V.F. Plyusnin, I.I. Blinov, K.P. Balashev, J. Photochem. Photobiol. A 51 (1990) 167.
[14] R.H. Compton, T.U. Gratton, T. Morrow, J. Photochem. 14 (1980) 61.
[15] I.M. Magin, V.S. Shevel'kov, A.A. Obynochny, A.I. Kruppa, T.V. Leshina, Chem. Phys. Lett. 357 (2002) 351–357.
[16] L. Láng, Absorption Spectra in the Ultraviolet and Visible Region, vol. 1, Academiai Kiado, Budapest, 1966, p. 93.
[17] H.V. Meek, C.V. Banks, Anal. Chem. 22 (1950) 1512.
[18] A.K. Babko, A.T. Pilipenko, Photometric Analysis: General Information and Apparatus, Khimiya, Moscow, 1968, p. 387 (in Russian).
[19] A.K. Pikaev, S.A. Kabakchi, I.E. Makarov, B.G. Ershov, Pulse Radiolysis and its Application, Atomizdat, Moscow, 1980, 280 pp. (in Russian).
[20] S.O. Nielsen, B.D. Michael, E.J. Hart, J. Phys. Chem. 80 (1976) 2482.
[21] B.D. Michael, E.J. Hart, K.H. Schmily, J. Phys. Chem. 75 (1971) 2802.
[22] Y.P. Tsentalovich, O.B. Morozova, A.V. Yurkovskaya, P.J. Hore, J. Phys. Chem. A 103 (1999) 5362–5368.
[23] K.M. Salikhov, Yu.N. Molin, R.Z. Sagdeev, A.L. Buchachenko, Spin Polarization and Magnetic Effects in Radical Reactions, Academiai Kiado, Budapest, 1984, 419 pp.
[24] A.C. Avery, J.R. Remko, B. Smaller, J. Chem. Phys. 49 (1968) 951.
[25] A.K. Pikaev, Solvated Electron in Radiation Chemistry, Nauka, Moscow, 1969, 457 pp. (in Russian).
[26] P. Neta, R.W. Fessenden, J. Phys. Chem. 78 (1974) 523.
[27] N.E. Polyakov, A.I. Kruppa, V.S. Bashurova, R.N. Musin, T.V. Leshina, E.S. Hand, L.D. Kispert, J. Photochem. Photobiol. A 129 (1999) 37.
[28] A.K. Pikaev, Modern radiation chemistry, in: Solids and Polymers: Applied Problems, Nauka, Moscow, 1987, 448 pp. (in Russian).
[29] G.V. Buxton, H.A. Gillis, N.V. Klassen, Can. J. Chem. 54 (1976) 367.
[30] A. Reuther, D.N. Nikogosyan, A. Laubereau, J. Phys. Chem. 100 (1996) 5570–5577.
[31] A. Migus, Y. Gauduel, J.L. Martin, A. Antonetti, Phys. Rev. Lett. 58 (1987) 1559–1562.
[32] Y. Kimura, J.C. Alfano, P.K. Walhout, P.F. Barbara, J. Phys. Chem. 98 (1994) 3450–3458.
[33] F.H. Long, H. Lu, K.B. Eisenthal, Phys. Rev. Lett. 64 (1990) 1469.
[34] R. Laenen, T. Roth, J. Mol. Struct. 598 (2001) 37–43.
[35] J.M. Wisenfeld, E.P. Ippen, Chem. Phys. Lett. 73 (1980) 47–49.
[36] D. Line, Handbook of Chemistry and Physics, 77th ed., CRC Press, Boca Raton, NY, 1996.
[37] D. Grand, A. Bernas, E. Amouyal, Chem. Phys. 41 (1973) 73.
[38] A.A. Oraevsky, D.N. Nikogosyan, Chem. Phys. 2 (1983) 1208 (in Russian).
[39] H. Lu, F.H. Long, R.M. Bowman, K.B. Eisenthal, J. Phys. Chem. 93 (1989) 27–28.
[40] D.N. Nikogosyan, A.A. Oraevsky, V.T. Rupasov, Chem. Phys. 77 (1983) 131.
[41] D.N. Nikogosyan, A.A. Oraevsky, V.S. Letokhov, Phys. Chem. 58 (1984) 1425–1427 (in Russian).
[42] J.L. McGowen, H.M. Ajo, J.Z. Zhang, B.Z. Schwartz, Chem. Phys. Lett. 231 (1994) 505–510.
[43] A. Iwata, N. Nakashima, Y. Izawa, C. Yamanaka, Chem. Lett. 21 (1993) 1939–1940.
[44] Kh.S. Bagdasaryan, Two-quantum Photochemistry, Nauka, Moscow, 1976, p. 128 (in Russian).
[45] Y. Gauduel, S. Pommeret, A. Migus, A. Antonetti, J. Chem. Phys. 93 (1989) 3880–3882.
[46] C.B. Amphlett, C.E. Adams, B.D. Michael, Adv. Chem. Ser. 81 (1968) 231–250.
[47] P. Neta, L.M. Dorfman, Adv. Chem. Ser. 81 (1968) 222–230.
[48] G.V. Buxton, C.L. Greenstock, W.P. Helman, A.B. Ross, J. Phys. Chem. Ref. Data 17 (1988) 559.
[49] V.E. Kogan, V.M. Fridman, V.V. Kafarov, Handbook of Solubility, vol. 1, No. 1, USSR Academy of Sciences, Moscow, 1962, p. 87 (in Russian).